Science of the Total Environment 955 (2024) 177084

Contents lists available at ScienceDirect

Science of the Total Environment

journal homepage: www.elsevier.com/locate/scitotenv

Short Communication

Imaging pollen using a Raspberry Pi and LED with deep learning

Ben Mills, Michalis N. Zervas, James A. Grant-Jacob *

Optoelectronics Research Centre, University of Southampton, Southampton, SO17 1BJ, UK

HIGHLIGHTS

- Current methods of pollen sensing are bulky and expensive.
- An LED and Raspberry Pi are used to reduce the cost of sensing.
- Lensless imaging and deep learning are used to image pollen grains.
- Pollen grains images were generated from their scattering patterns.
- Imaging pollen using a Raspberry Pi, LED and deep learning can be achieved for ~£100.

GRAPHICAL ABSTRACT

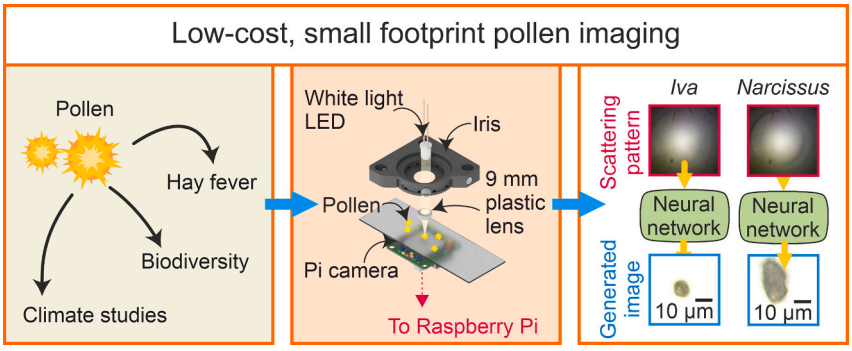

ARTICLE INFO

Editor: Alessandra De Marco

Keywords:
AI
Imaging
Palynology
Bioaerosols
Sensing
Pollen grains

ABSTRACT

The production of low-cost, small footprint imaging sensor would be invaluable for airborne global monitoring of pollen, which could allow for mitigation of hay fever symptoms. We demonstrate the use of a white light LED (light emitting diode) to illuminate pollen grains and capture their scattering pattern using a Raspberry Pi camera. The scattering patterns are transformed into 20× microscope magnification equivalent images using deep learning. We show the ability to produce images of pollen from plant species previously unseen by the neural network in training. Such a technique could be applied to imaging airborne particulates that contribute to air pollution, and could be used in the field of environmental science, health science and agriculture.

1. Introduction

Pollen allergies, also known as hay fever, are a significant health concern, affecting an estimated 26 % of adults in the United Kingdom (UK) (Scadding et al., 2017), with prevalence been shown to be increasing in Denmark over the past 20 years (Leth-Møller et al., 2020), and economic cost being €195.6 patient/year in China (Li et al., 2022). These allergies can have a substantial impact on an individual's health, especially during the spring and summer months (Bauchau and Durham, 2004). Whilst only specific pollen producing plants cause hay fever, the local pollen count can aid in the mitigation of hay fever symptoms, as it gives an indication of potential levels of overall pollen in the air. However, these counts generally do not consider pollen of plant species, which can have degrees of allergenicity (Osborne et al., 2017; Caillaud et al., 2014). Therefore, the development of a real-time sensor that can identify and quantify pollen of different plant species at a specific

* Corresponding author.
E-mail address: J.A.Grant-Jacob@soton.ac.uk (J.A. Grant-Jacob).

https://doi.org/10.1016/j.scitotenv.2024.177084
Received 19 June 2024; Received in revised form 17 October 2024; Accepted 18 October 2024
Available online 19 October 2024

location would be extremely beneficial. Although the plant species that produce pollen that can lead to hay fever is still unclear (Sousa-Silva et al., 2021), and individuals suffering from hay fever should seek medical advice to discover more about their allergies, such a device could aid individuals in identifying the specific plant taxa causing their severe symptoms or even avoid exposure to these pollens. In addition to its health benefits, monitoring pollen levels can also provide valuable information about the climate (Newnham et al., 2013), insect migration patterns (Suchan et al., 2019), and crop production (Fernandez-Mensaque et al., 1998).

Currently, the techniques available for real-time sensing of pollen grains are limited in temporal and spatial resolution. Whilst optical particle counters can detect particles of a certain size in real-time, they cannot identify the species of particle (i.e., smoke, pollen, cement dust) (Grant-Jacob and Mills, 2022). Pollen collected using Burkard traps (Levetin et al., 2000) (kettle-sized traps or larger depending on type) requires subsequent laboratory analysis to determine the family or species (Pashley et al., 2015). Some analysis techniques can identify pollen up to plant species level whereas others do not go further than family or genus. Light microscopy techniques often only allow identification up to the family or genus level, since many pollen grains have similar morphological characteristics, making it difficult to distinguish between species within the same family or genus. Acetolysis is a technique used to process pollen and prepare it for morphological identification via light microscopy (Warcup and Roberton, 2023), by removing unwanted substances from the grains, revealing important morphological features of the grains. Pollen grains can also be stained prior to light microscopy analysis to allow better contrast with the background, providing greater detail of the exine and ornamentation (Alexander, 1980). FTIR (Fourier Transform Infrared Spectroscopy) is a method that uses infrared light to observe chemical properties of pollen grains and can help in distinguishing between different taxa, and even species in some cases (Zimmermann and Kohler, 2014). Another method, DNA (deoxyribonucleic acid) Metabarcoding utilises DNA extraction, sequencing, and analysis for plant species level identification of pollen (Sickel et al., 2015).

Recently, automated methods for identifying pollen from traps have been developed using light-based techniques such as optical and laser-based fluorescence imaging (Kawashima et al., 2017; Schiele et al., 2019; Crouzy et al., 2016; Mitsumoto et al., 2009). However, these devices can be quite large, and so a sensor capable of imaging a pollen grain with cost-effective and minimal optics, and with a small footprint (such as a lensless-based Raspberry Pi (Grant-Jacob et al., 2019a)) would be invaluable for mass deployment in practice on a national or international scale. A method that uses minimal optics is lensless imaging, which images via capturing and processing the light scattered from an object (i.e., the image of its scattering pattern). This scattering pattern image contains information about the object's morphology and chemical composition (Bohren and Huffman, 2008; Wiscombe, 1980), and can be converted into an image of the sample using methods such as phase retrieval and ptychography (Maiden et al., 2011; Fienup, 1982; Pfeiffer et al., 2006), or more recently using deep learning neural networks (Grant-Jacob et al., 2020; Nguyen et al., 2018; Goy et al., 2018; Kemp, 2018).

The capability of airborne imaging of pollen would allow plant pollen family verification, and identification of the size and shape of pollen (all of which are useful for understanding crop health and the environment). For example, a study suggests that pollen grain size could potentially be used as a proxy for long-term climate change (Griener and Warny, 2015), particularly in relation to changes in moisture availability. Another study found that both soil fertility and mycorrhizal infection had significant effects on the male traits of the plants, including pollen production and pollen grain size (Lau et al., 1995), suggesting that changes in the environment, such as nutrient availability in the soil, could influence the characteristics of pollen.

Whilst deep learning convolutional neural networks (CNNs) have been successful in identifying pollen from scattering patterns (Grant-Jacob et al., 2018; Grant-Jacob et al., 2019b), these works involve the use of CNNs for identification and not for image generation. The setups in the papers included the use of expensive imaging cameras (~£500 each) to capture the scattering patterns, and so a cheaper camera such as a Raspberry Pi camera (~£50) would be more desirable. In addition, these previous works used lasers for creating scattering patterns in lensless imaging, but a cheaper light source like an LED (light emitting diode) could enable even lower cost sensing (potentially 100× lower cost for the light source). In general, lasers are used for lensless imaging due to their higher spatial coherence, which provides diffraction patterns with structure that the deep learning neural networks can interpret. In this work, we use a white light LED coupled with an aperture (for spatial filtering of the light), to produce a scattering pattern from the pollen grains onto a Raspberry Pi camera sensor and subsequently use deep learning to transform that scattering pattern into an image of the pollen grain. Different from CNNs, we use a conditional generative adversarial network (cGAN), which rather than reduces an image to a single or vector output, such architecture is a U-Net structure such that it reduces the image, but then increases it again to an image the same size as the input, transforming it in the process. The ability to link a scattering pattern from a pollen grain to its microscope image negates the need to produce microscope images, thus significantly reducing costs and saving time. Critically, the ability to image a pollen grain can allow for shape, size, and colour of the pollen grains to be determined, in addition to identification of the species producing the pollen.

2. Materials and methods

2.1. Sample preparation

The taxa used in this experiment were pollen that had a variety of shapes and sizes (to allow the neural network to learn from a diverse dataset) and were available on the University of Southampton campus or available to order. *Iva xanthiifolia* and *Populus deltoides* pollen grains were procured from Sigma Aldrich. *Allium ursinum*, *Narcissus pseudonarcissus*, *Tulipa saxatilis*, *Ranunculus repens* and *Taraxacum officinale* pollen grains were collected from the campus. From this point forward, we shall only use the genus of the plant for ease of reading. Two substrates (25 mm × 75 mm × 1 mm thick pre-cleaned soda-lime glass slide by J. Melvin Freed Brand) were used. These glass slides were cleaned using acetone and lens tissue, and allowed to dry before pollen from each species was sequentially deposited onto them using a laboratory grade cotton bud (RS.com). The pollen grains were sprinkled over the surface of the glass slide, covering approximately a 25 mm × 25 mm area, at a density of ~3 pollen per mm^2. The pollen used were dry and did not contain any staining chemicals, nor was acetolysis used. *Iva*, *Populus*, *Narcissus* and *Ranunculus* pollen grains were deposited onto the first substrate (for neural network training and testing), whilst *Tulipa*, *Allium* and *Taraxacum* pollen grains were deposited onto the second substrate (for neural network testing only).

2.2. Experimental setup

The experimental setup is presented in Fig. 1a). To image the pollen grains, we used a Nikon ECLIPSE LV150L with a 20× Nikon objective (NA = 0.4, WD = 13 mm), a 10× ocular lens, a 0.55× TV lens and a colour camera (Basler acA3088-57uc, 6MP IMX178 sensor, 3088 × 2064 pixels, RGB), giving a 110× total image magnification. A pollen covered glass slide was attached to motorized XYZ Zaber stages (Zaber X-LSM050A-E03, X-LSM100A, X-VSR20A-E01) that could translate the pollen beneath the microscope in a raster scanning motion in X and Y to acquire images, and could then translate to the Raspberry Pi scattering setup. The step size of the X and Y stages was 0.047 μm, having an accuracy of 15 μm, repeatability of <3 μm. The Raspberry Pi setup illumination/scattering *Z*-axis was approximately 85 mm away from the

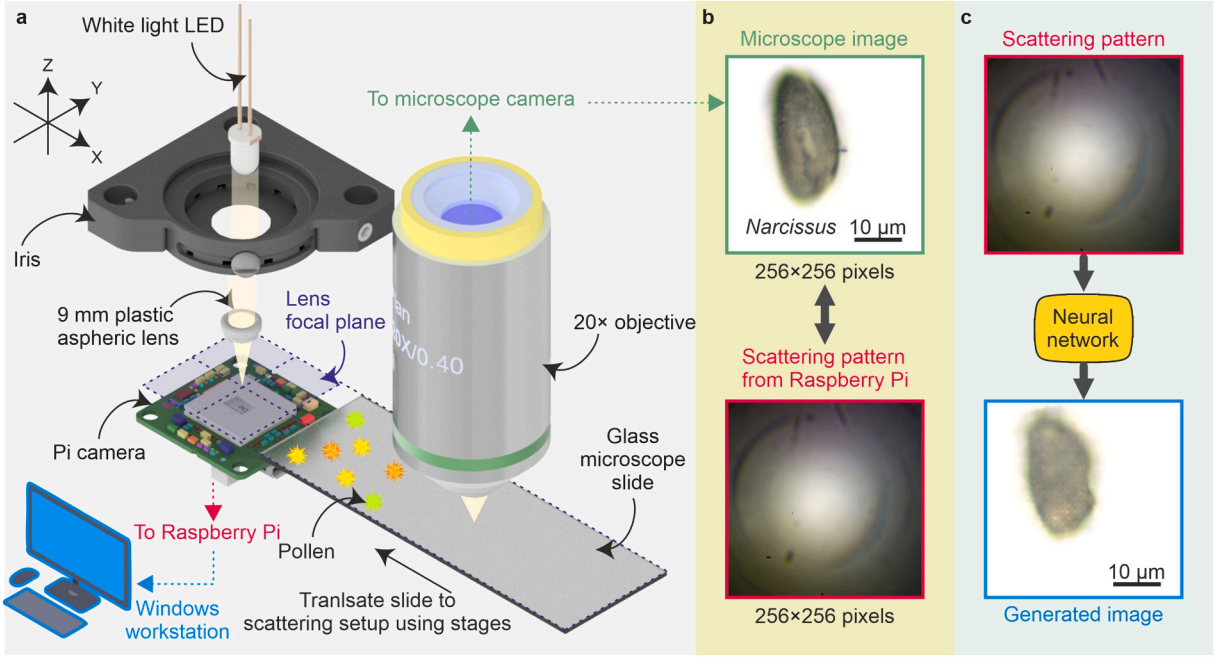

Fig. 1. A) Diagram of experimental setup showing the imaging setup consisting of a 20× microscope objective connected to a microscope, next to the Raspberry Pi-based sensing setup. The pollen covered glass microscope slide was translated between setups using motorized XYZ stages. B) Example of a microscope image (green outline) from the imaging setup and associated scattering pattern (red outline) captured by the Pi camera from the sensing setup. c) Schematic of transforming scattering pattern (red outline) using a neural network (yellow box), trained on a Windows workstation, into a generated image of the pollen grains (blue outline).

centre of the microscope imaging Z-axis. This combination of two adjacent experimental systems allowed the collection of both microscope images of the sample and the associated scattering patterns, which was key for training the neural network to transform scattering patterns into microscope images. However, it is important to realize that whilst two systems were used here, once the neural network is trained, only the low-cost Raspberry Pi sensor system would be needed for in practice implementation. As demonstrated in previous work, the Raspberry Pi itself could also run the trained neural network (Grant-Jacob et al., 2019a). This means that one can duplicate the Raspberry Pi setup for capturing scattering patterns, and transform the scattering patterns into microscope images without the need for an expansive microscope (~£10,000), or even microscope objectives (~£1000) to image the pollen grains.

The Raspberry Pi sensor setup consisted of a white light LED. The LED was followed by an aperture (<1 mm diameter) placed approximately 2 cm after the end of the LED to spatially filter the light from the LED, and therefore enhance the fringe visibility in the scattering patterns, hence enhancing the likelihood of a neural network being able to transform a scattering pattern image correctly into an image of the pollen grain. Following this, the light was focused onto a pollen grain using a moulded plastic aspheric lens (6 mm, NA = 0.38), and the light scattered from the pollen grain was then captured using an HQ Pi camera (4056 × 3040 pixels, RGB), which was connected to a Raspberry Pi 4. The Raspberry Pi scattering setup cost approximately £100.

Data from the Raspberry Pi camera were acquired remotely via an ethernet cable connected to a Dell Precision 7865 Windows 10 workstation consisting of an Intel(R) Xeon(R) Gold 5222 CPU @ 3.80GHz 3.79 GHz (2 processors) and 3× NVIDIA RTX A4500 (20 GB VRAM, 184 tensor cores each) graphics processing unit (GPU). The workstation also controlled the Zaber XYZ stages and the microscope's Basler camera. The stages and imaging of both the Basler and Pi cameras was automated using Python code.

2.3. Data collection

The first sample was raster scanned using the XYZ stages beneath the objective over a total of approximately 500 mm^2. Each raster scanning step was 550 μm to minimise any overlapping of images and minimise the time of data collection. Individual and agglomerated pollen grains were located and imaged such that each pollen grain was at the centre of the camera sensor, after which the images were cropped. The corresponding scattering patterns were collected for training and testing of the neural network. The images of the scatting patterns were cropped to 1024 × 1024 pixels then resized to 256 × 256 pixels to match the size of the cropped microscope images. Subsequently, the pollen grains from the second slide were imaged and scattering patterns were recorded, purely to test the capability of the neural network to generate images of not just unseen pollen grains but pollen grains from previously unseen plant species. In total, 1800 images were collected, but agglomeration of pollen grains that extended beyond the cropped and resized 256 × 256 pixels image size were discarded. As such, 935 pairs of images (microscope image and scattering pattern) were used for training and 31 used for testing from the first slide with 100 used for testing from the second slide.

A total of 935 pollen images and scattering patterns (divided over 4 different species, *Iva*, *Populus*, *Narcissus* and *Ranunculus*) from the first slide were used to train the neural network (see Table 1). The number of plants that *Iva* and *Populus* were collected from is unknown as they were purchased from Sigma Aldrich, but since the bottles are 1 g and 500 mg, respectively, to obtain such a quantity of pollen would require pollen to be sourced from a large quantity of flowers. Pollen was collected from 4× *Ranunculus*, 4× *Taraxacum*, 3× *Tulipa*, 3× *Allium*. However, whilst multiple flowers were collected, due to the sparsity of such pollen from the plants, the numbers used in training and testing were low. It should be noted that some pollen grains were fragmented, and blank images were also included in the data, hence have been assigned the unknown column in Table 1. Even though more pollen from *Iva* were used in training, and it has been shown that a varied dataset is necessary for overfitting (Li et al., 2023), the key part for accurate image generation is

Table 1
Number of pollen grains from each plant species used in training and testing the neural network.

	Ranunculus	*Populus*	*Narcissus*	*Iva*	*Tulipa*	*Allium*	*Taraxacum*	*Unknown*
Training	91	47	137	650	0	0	0	10
Testing	5	2	10	13	47	30	23	1

to have enough varied data, such as pollen grains of different orientation, sizes and agglomerations. The pollen size distribution of the training data was calculated by binarizing the images and calculating the white pixels that represented the pollen. This showed that pollen grains in the training set had a distribution with a mean area of 2341.8 pixels^2 (383.3 μm^2) and a standard deviation of 1757 pixels^2 (287.6 μm^2), indicating significant variability. The distribution is strongly right-skewed (skewness = 1.95) with heavy tails (kurtosis = 7.63), suggesting the presence of large outliers. A lognormal distribution with parameters $\mu = 5.24$ and $\sigma = 3.46$ provides a good fit to the data, which is typical for naturally occurring size distributions. Table 1 shows the number of pollen grains from different species used in training and testing.

2.4. Neural network

Deep learning CNNs are designed to mimic the visual cortex and use convolutional layers to process features in images. They have proven to be very successful at identifying objects in images, and have been used in the automatic identification of pollen in images (Li et al., 2023; Polling et al., 2021). Unlike CNNs, we utilise a cGAN with a U-Net architecture that is designed to transform one image to another. We used a cGAN

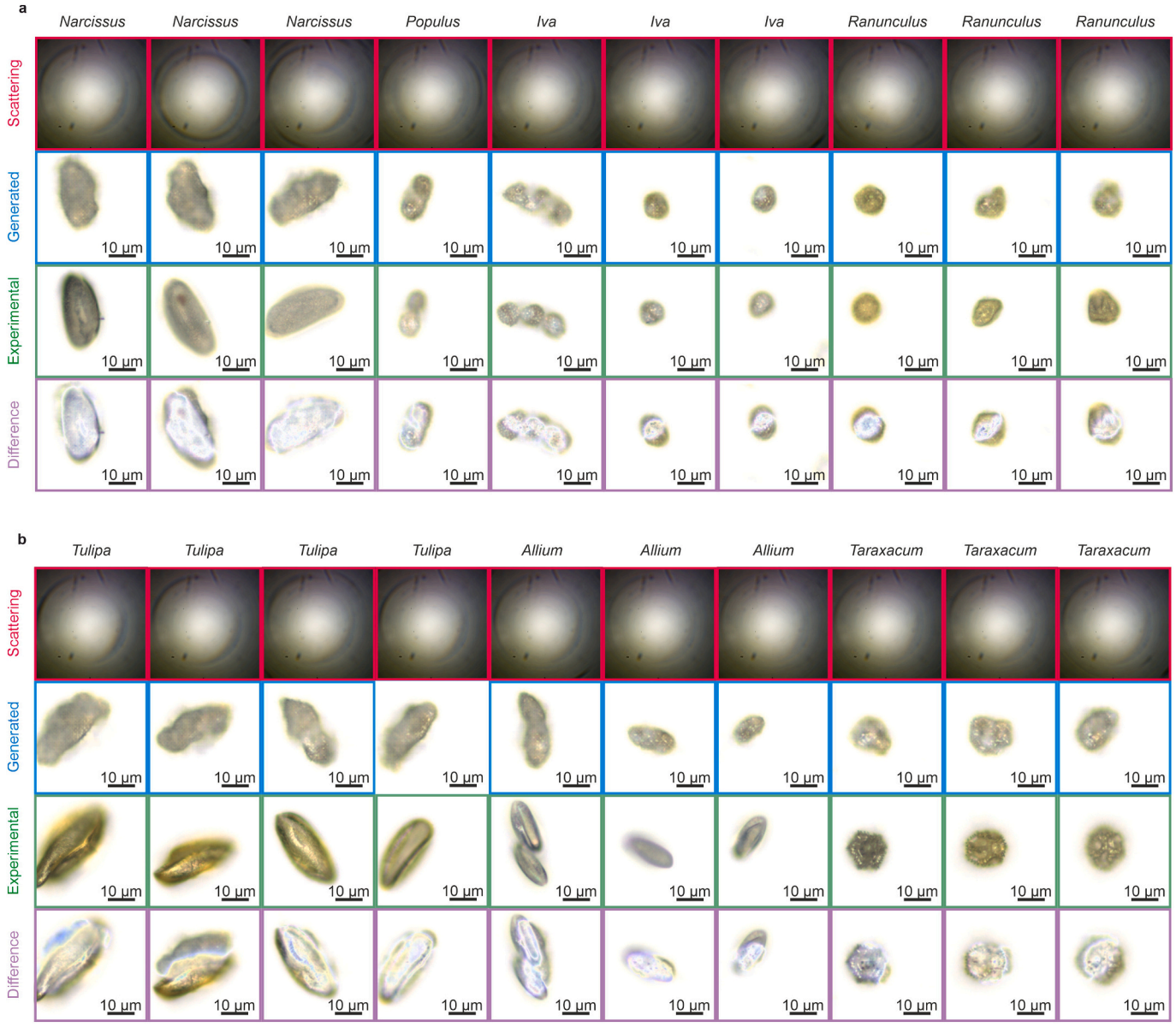

Fig. 2. Capability of the neural network on previously unseen pollen (*Narcissus Populus, Iva* and *Ranunculus*), and on previously unseen pollen from different plant species (*Tulipa*, *Alliium* and *Taraxacum*). The first row shows the scattering pattern, the second row shows the generated image, the third shows the experimental image, and the fourth shows the difference, where the darker pixels indicate regions of greater error.

architecture known as Pix2pix (Isola et al., 2017), using a workstation running Windows 10 and equipped with an AMD Ryzen Threadripper PRO 5975WX and two NVIDIA A6000 GPUs (48 GB VRAM each). The cGAN framework described and illustrated in more detail in (Grant-Jacob et al., 2021) had a generator network with a 7-layer architecture in order to enable an image resolution of 256 × 256 pixels and had a learning rate of 0.0002 and drop-out of 0.5. At the start of training, the neuron weightings for the generator were randomly, meaning they encoded no information about the training data (experimental images).

The neural network was trained for 160 epochs until the training errors reached a minimum, which took nearly 3 h. A total of 935 pollen images and scattering patterns from the first slide were used to train the neural network. The neural network was then applied to 31 scattering patterns from the first slide not used in training. The neural network outputted generated images of pollen grains, and were compared to the experimentally obtained pollen images. To further test the capability of the neural network, we used 100 scattering patterns collected from pollen grains on the second slide, since no pollen grains from these plant species were used in training, and therefore structures of the pollen grains would not have been seen by the neural network in training. This illustrates that the neural network has not overfitted to the specific scattering patterns it was trained on but has developed a generalized understanding that features in the scattering patterns correspond to features in the images of pollen grains, hence enabling it to accurately recognise and relate features across different examples. Therefore, the successful generation of images of previously unseen pollen species demonstrates the robustness of the network.

3. Results and discussion

Fig. 2a displays the 10 results of testing the neural network on previously unseen pollen (*Narcissus*, *Populus, Iva* and *Ranunculus*), whilst Fig. 2b shows the results of testing the neural network on 10 pollen grains from previously unseen plant species (*Tulipa*, *Allium* and *Taraxacum*). The first row shows the experimental scattering pattern, the second row shows the images generated by the neural network, the third row shows the experimental image, and the fourth row shows the difference between rows two and three (RGB pixel intensity in generated image minus RGB pixel intensity in experimental image). Since the image has been inverted for ease of viewing, the darker pixels (low intensity pixel value) indicate regions of greater error. As seen in the figure, the quantity of the pollen grains in each generated image is correct, as in the case for *Iva* there being 3 in one instance, and *Populus* and *Allium* being two, and one pollen for all the others. The orientation and size of pollen grains in the generated images are very similar, as can be seen in the difference images in the fourth row. Whilst the size and orientation are generally correct, the surface texture is generally not. This is perhaps due to the higher spatial frequency information contained in the scattering pattern not being distinguishable (and thus extractable) due to low spatial coherence of the light source.

Table 2 displays the Structural Similarity Index Measure (1 being exactly the same, 0 indicating no similarity and 1 being completely anti-correlated), Peak Signal-to-Noise Ratio (PSNR) (higher the value the more accurate the generated image), Mean Squared Error (MSE) (lower value the greater the similarity) of the generated images compared with the experimental images and Perceptual Image Quality Evaluator (PIQE), which provides a no-reference metric based on perceptual image quality (a smaller score indicates better perceptual quality).

The SSIM assesses the visual impact of image contrast, luminance and structure, and was determined using the following formula,

$$SSIM(E,G) = \frac{(2\mu_E\mu_G + C_1)(2\sigma_{EG} + C_2)}{(\mu_E^2 + \mu_G^2 + C_1)(\sigma_E^2 + \sigma_G^2 + C_2)}$$

where μ_E is the mean of E, μ_G is the mean of G, σ_E^2 is the variance of E, σ_G^2 is the variance of G, σ_{EG} is the covariance of E and G, $C_1 = (0.01\ L)^2$ and $C_2 = (0.03\ L)^2$, where L is the dynamic range of the pixel values.

The PSNR equation used was,

$$PSNR = 10log_{10}\left(\frac{max^2(E,G)}{\frac{1}{N\times M}\sum_{M,N}(E(m,n) - E(m,n))^2}\right)$$

where N and M are the total number of rows and columns of pixels in the images, max(E,G) is the maximum intensity value of the experimental image E and the generated image G, and m and n are the pixels in each row and column.

The mean square error (MSE) was determined by taking the average of the squared intensity differences between each pixel in the generated image (with intensity values in the 0–255 range) and the corresponding pixel in the experimental image (also with intensity values in the 0–255 range),

$$MSE = \frac{1}{N}\sum_{i=1}^{N}(G_i - E_i)^2$$

where N is the number of data points (pixels), G_i is the generated pixel value and E_i is the actual pixel value, E_{imax} is the maximum pixel value and E_{imin} is the minimum pixel value of the experimental image.

The PIQE does not have a simple, closed-form mathematical formula like the MSE, PSNR and SSIM used for full-reference methods, but instead works by analysing localized distortion such as blocking artifacts, blur and noise. We use MATLAB's in built "piqe" found in the "Image Processing Toolbox" (Venkatanath et al., 2015). The average SSIM for all 131 test data was 0.88, whilst the average PSNR was 21.4 and the average MSE was 835. Any artifact to the edge of the images might not be accurately reconstructed as limited information associated with this defect might not have been contained in the scattering pattern due to the size of the LED beam. It is also evident that the colour of the generated images is generally similar to that of the experimental microscope images, i.e., either yellow or grey. The SSIM value is high likely due to the large number of white pixels in the background of the images. However, it is still important to generate this background correctly. The average PIQE value was 35.2 for all images, indicating good image quality. More specifically in Table 2, *Narcissus*, *Populus, Tulipa* and *Taraxacum* images had good quality, whilst *Allium* images had fair image quality on average.

The ability to image pollen could allow more precise identification and pollen morphological analysis, and such a technique could extend to other bioaerosols or airborne particulates. Since testing data was acquired remotely via an ethernet cable, this technique could be extended to using wireless technology, which the Raspberry Pi already has, and could be extended for use in real-time with the use of a flow chamber (Wang and Muth, 2017) or an impactor on the surface of a glass slide (Luo et al., 2022). The low cost of the proof-of-principle imaging sensor

Table 2
SSIM, PSNR and MSE for the generated and experimental pollen images shown in Fig. 2 (the number of pollen grain images for each species is indicate in brackets).

	Ranunculus (3)	*Populus* (1)	*Narcissus* (3)	*Iva* (3)	*Tulipa* (4)	*Allium* (3)	*Taraxacum (3)*
SSIM	0.94	0.79	0.89	0.93	0.85	0.92	0.91
PSNR	23.8	12.9	22.4	24.2	18.2	23.0	21.1
MSE	274.5	3358.0	447.0	247.6	1222.5	512.8	517.9
PIQE	33.6	17.7	21.0	35.2	26.7	41.2	20.8

(~£100) could be taken up by industry where costs could be reduced further.

4. Conclusion

Using a white LED, aperture and a Raspberry Pi camera, we demonstrated the possibility of using deep learning to transform images of the LED light scattered from a pollen grain to that of an image of a pollen grain captured using a 20× magnification objective. We were able to show the reconstruction of pollen grain shape and orientation of pollen from plant species used in training such as *Populus* and *Ranunculus*, and of pollen from plant species exempt from training, such as *Tulipa* and *Allium*. The low-cost sensing technique demonstrated here could be applied to airborne pollen grains and pave the way to cheap imaging sensors for pollen and airborne particulates.

CRediT authorship contribution statement

Ben Mills: Writing – review & editing, Resources. **Michalis N. Zervas:** Writing – review & editing, Funding acquisition. **James A. Grant-Jacob:** Writing – review & editing, Writing – original draft, Visualization, Software, Project administration, Methodology, Investigation, Formal analysis, Data curation, Conceptualization.

Declaration of competing interest

The authors declare that they have no known competing financial interests or personal relationships that could have appeared to influence the work reported in this paper.

Acknowledgments

The study was financed by the Engineering and Physical Sciences Research Council (EPSRC) grant no. EP/T026197/1, EP/W028786/1.

Data availability

Data for this article are available at https://doi.org/10.5258/SOTON/D3107.

References

Alexander, M.P., 1980. A versatile stain for pollen fungi, yeast and bacteria. Stain Technol. 55 (1), 13–18.
Bauchau, V., Durham, S.R., 2004. Prevalence and rate of diagnosis of allergic rhinitis in Europe. Eur. Respir. J. 24 (5), 758–764.
Bohren, C.F., Huffman, D.R., 2008. Absorption and Scattering of Light by Small Particles. John Wiley & Sons.
Caillaud, D., Martin, S., Segala, C., Besancenot, J.-P., Clot, B., Thibaudon, M., 2014. Effects of airborne birch pollen levels on clinical symptoms of seasonal allergic Rhinoconjunctivitis. Int. Arch. Allergy Immunol. 163 (1), 43–50.
Crouzy, B., Stella, M., Konzelmann, T., Calpini, B., Clot, B., 2016. All-optical automatic pollen identification: towards an operational system. Atmos. Environ. 140, 202–212.
Fernandez-Mensaque, P.C., Minero, F.J.G., Morales, J., Tomas, C., 1998. Forecasting olive (Olea europaea) crop production by monitoring airborne pollen. Aerobiologia (Bologna) 14 (2), 185–190.
Fienup, J.R., 1982. Phase retrieval algorithms: a comparison. Appl. Optics 21 (15), 2758–2769.
Goy, A., Arthur, K., Li, S., Barbastathis, G., 2018. Low photon count phase retrieval using deep learning. Phys. Rev. Lett. 121 (24), 243902.
Grant-Jacob, J.A., Everitt, C., Eason, R.W., King, L.J., Mills, B., 2021. Exploring sequence transformation in magnetic resonance imaging via deep learning using data from a single asymptomatic patient. J Phys Commun 5 (9), 95015.
Grant-Jacob, J.A., Jain, S., Xie, Y., Mackay, B.S., McDonnell, M.D.T., Praeger, M., Loxham, M., Richardson, D.J., Eason, R.W., Mills, B., 2019b. Fibre-optic based particle sensing via deep learning. Journal of Physics: Photonics 1 (4), 44004.
Grant-Jacob, J.A., Mackay, B.S., Baker, J.A.G., Heath, D.J., Xie, Y., Loxham, M., Eason, R. W., Mills, B., 2018. Real-time particle pollution sensing using machine learning. Opt. Express 26 (21), 27237–27246.
Grant-Jacob, J.A., Mills, B., 2022. Deep learning in airborne particulate matter sensing: a review. J Phys Commun 6 (12), 122001.
Grant-Jacob, J.A., Praeger, M., Loxham, M., Eason, R.W., Mills, B., 2020. Lensless imaging of pollen grains at three-wavelengths using deep learning. Environ Res Commun 2 (7), 075005.
Grant-Jacob, J.A., Xie, Y., Mackay, B.S., Praeger, M., McDonnell, M.D.T., Heath, D.J., Loxham, M., Eason, R.W., Mills, B., 2019a. Particle and salinity sensing for the marine environment via deep learning using a raspberry pi. Environ Res Commun 1 (3), 035001.
Griener, K.W., Warny, S., 2015. Nothofagus pollen grain size as a proxy for long-term climate change: an applied study on Eocene, Oligocene, and Miocene sediments from Antarctica. Rev. Palaeobot. Palynol. 221, 138–143.
Isola, P., Zhu, J.-Y., Zhou, T., Efros, A.A., 2017. Image-to-image translation with conditional adversarial networks. In: In *2017 IEEE Conference on Computer Vision and Pattern Recognition (CVPR)*. IEEE, pp. 5967–5976.
Kawashima, S., Thibaudon, M., Matsuda, S., Fujita, T., Lemonis, N., Clot, B., Oliver, G., 2017. Automated pollen monitoring system using laser optics for observing seasonal changes in the concentration of total airborne pollen. Aerobiologia (Bologna) 33 (3), 351–362.
Kemp, Z.D.C., 2018. Propagation based phase retrieval of simulated intensity measurements using artificial neural networks. J. Opt. 20 (4), 45606.
Lau, T.-C., Lu, X., Koide, R.T., Stephenson, A.G., 1995. Effects of soil fertility and mycorrhizal infection on pollen production and pollen grain size of Cucurbita pepo (Cucurbitaceae). Plant Cell Environ. 18 (2), 169–177.
Leth-Møller, K.B., Skaaby, T., Linneberg, A., 2020. Allergic rhinitis and allergic sensitisation are still increasing among Danish adults. Allergy 75 (3), 660–668.
Levetin, E., Rogers, C.A., Hall, S.A., 2000. Comparison of pollen sampling with a Burkard spore trap and a Tauber trap in a warm temperate climate. Grana 39 (6), 294–302.
Li, C., Polling, M., Cao, L., Gravendeel, B., Verbeek, F.J., 2023. Analysis of automatic image classification methods for Urticaceae pollen classification. Neurocomputing 522, 181–193.
Li, X., Xu, X., Li, J., Huang, Y., Wang, C., Zhang, Y., Zhang, L., 2022. Direct and indirect costs of allergic and non-allergic rhinitis to adults in Beijing, China. Clin. Transl. Allergy 12 (4), e12148.
Luo, Y., Zhang, Y., Liu, T., Yu, A., Wu, Y., Ozcan, A., 2022. Virtual impactor-based label-free pollen detection using holography and deep learning. ACS Sens 7 (12), 3885–3894.
Maiden, A.M., Humphry, M.J., Zhang, F., Rodenburg, J.M., 2011. Superresolution imaging via ptychography. JOSA A 28 (4), 604–612.
Mitsumoto, K., Yabusaki, K., Aoyagi, H., 2009. Classification of pollen species using autofluorescence image analysis. J. Biosci. Bioeng. 107 (1), 90–94.
Newnham, R.M., Sparks, T.H., Skjøth, C.A., Head, K., Adams-Groom, B., Smith, M., 2013. Pollen season and climate: is the timing of birch pollen release in the UK approaching its limit? Int. J. Biometeorol. 57 (3), 391–400.
Nguyen, T., Xue, Y., Li, Y., Tian, L., Nehmetallah, G., 2018. Deep learning approach for Fourier ptychography microscopy. Opt. Express 26 (20), 26470–26484.
Osborne, N.J., Alcock, I., Wheeler, B.W., Hajat, S., Sarran, C., Clewlow, Y., McInnes, R. N., Hemming, D., White, M., Vardoulakis, S., Fleming, L.E., 2017. Pollen exposure and hospitalization due to asthma exacerbations: daily time series in a European city. Int. J. Biometeorol. 61 (10), 1837–1848.
C. H. Pashley, J. Satchwell, and R. E. Edwards, "Ragweed pollen: is climate change creating a new aeroallergen problem in the UK?," (2015).
Pfeiffer, F., Weitkamp, T., Bunk, O., David, C., 2006. Phase retrieval and differential phase-contrast imaging with low-brilliance X-ray sources. Nat. Phys. 2, 258–261.
Polling, M., Li, C., Cao, L., Verbeek, F., de Weger, L.A., Belmonte, J., De Linares, C., Willemse, J., de Boer, H., Gravendeel, B., 2021. Neural networks for increased accuracy of allergenic pollen monitoring. Sci. Rep. 11 (1).
G. K. Scadding, H. H. Kariyawasam, G. Scadding, R. Mirakian, R. J. Buckley, T. Dixon, S. R. Durham, S. Farooque, N. Jones, S. Leech, S. M. Nasser, R. Powell, G. Roberts, G. Rotiroti, A. Simpson, H. Smith, and A. T. Clark, "BSACI guideline for the diagnosis and management of allergic and non-allergic rhinitis (Revised Edition 2017; First edition 2007)," Clinical & Experimental Allergy 47(7), 856–889 (2017).
J. Schiele, F. Rabe, M. Schmitt, M. Glaser, F. Haring, J. O. Brunner, B. Bauer, B. Schuller, C. Traidl-Hoffmann, and A. Damialis, "Automated Classification of Airborne Pollen using Neural Networks," in *2019 41st Annual International Conference of the IEEE Engineering in Medicine and Biology Society (EMBC)* (2019), 2019, pp. 4474–4478.
Sickel, W., Ankenbrand, M.J., Grimmer, G., Holzschuh, A., Härtel, S., Lanzen, J., Steffan-Dewenter, I., Keller, A., 2015. Increased efficiency in identifying mixed pollen samples by meta-barcoding with a dual-indexing approach. BMC Ecol. 15 (1), 20.
Sousa-Silva, R., Smargiassi, A., Kneeshaw, D., Dupras, J., Zinszer, K., Paquette, A., 2021. Strong variations in urban allergenicity riskscapes due to poor knowledge of tree pollen allergenic potential. Sci. Rep. 11 (1), 10196.
Suchan, T., Talavera, G., Sáez, L., Ronikier, M., Vila, R., 2019. Pollen metabarcoding as a tool for tracking long-distance insect migrations. Mol. Ecol. Resour. 19 (1), 149–162.
N. Venkatanath, D. Praneeth, M. C. Bh, S. S. Channappayya, and S. S. Medasani, "Blind image quality evaluation using perception based features," in *2015 Twenty First National Conference on Communications (NCC)* (2015), pp. 1–6.
Wang, Y., Muth, J.F., 2017. An optical-Fiber-based airborne particle sensor. Sensors (Basel) 17 (9), 2110.
Warcup, K., Roberton, B., Kral-O'Brien, K., Harmon, J., 2023. Acetolysis modifications to process small pollen samples swabbed from live bees. J. Insect Sci. 23 (6), 1.
Wiscombe, W.J., 1980. Improved Mie scattering algorithms. Appl. Optics 19 (9), 1505–1509.
B. Zimmermann and A. Kohler, "Infrared spectroscopy of pollen identifies plant species and genus as well as environmental conditions," PloS One 9(4), e95417- (2014).